Advances in Science and Technology Research Journal

Advances in Science and Technology Research Journal, 2026, 20(10), 168–179
https://doi.org/10.12913/22998624/224607
ISSN 2299-8624, License CC-BY 4.0

Received: 2026.04.09
Accepted: 2026.07.15
Published: 2026.09.01

Influence of supersaturation temperature on microstructure and tensile properties of austenitic twinning-induced plasticity steel

Marek Opiela[1*], Gabriela Fojt-Dymara[2], Barbara Grzegorczyk[1], Krzysztof Matus[3]

[1] Department of Engineering Materials and Biomaterials, Faculty of Mechanical Engineering, Silesian University of Technology, ul. Konarskiego 18A, 44-100 Gliwice, Poland
[2] Department of Engineering Processes Automation and Integrated Manufacturing Systems, Faculty of Mechanical Engineering, Silesian University of Technology, ul. Konarskiego 18A, 44-100 Gliwice, Poland
[3] Materials Research Laboratory, Faculty of Mechanical Engineering, Silesian University of Technology, ul. Konarskiego 18A, 44-100 Gliwice, Poland
* Corresponding author's e-mail: marek.opiela@polsl.pl

ABSTRACT

The paper presents a detailed assessment of the influence of supersaturation temperature on the development of the microstructure and mechanical properties of high-manganese austenitic twinning-induced plasticity (TWIP) steel. Particular attention was paid to the analysis of changes occurring in the material's structure and their direct impact on the strength and plasticity parameters depending on the applied treatment temperature. The average austenite grain diameter after supersaturation in water from 900 °C to 1100 °C changes from about 15 μm to about 132 μm. The static tensile test showed that the mechanical properties of the tested TWIP steel after supersaturation within a given temperature range changed as follows: yield strength ($YS_{0.2}$) from 485 MPa to 345 MPa, ultimate tensile strength (UTS) from 797 MPa to 656 MPa, elongation (UEl) from 39% to 49%, and reduction in area (RA) from 43% to 51%. Transmission electron microscopy studies allowed identifying (Ti,Nb)C and (Ti,Nb)(C,N) precipitations, mainly located at the austenite grain boundaries, ensures fine-grained microstructure. Microstructure observations with the use of X-ray and EBSD techniques, after supersaturation of the samples and their subsequent tensile testing, also showed the presence of ε martensite, the average content of which – regardless of the supersaturation temperature – was approximately 8%. In the investigated steel, the presence of non-metallic inclusions was also revealed, mainly of the oxide–sulfide type, with an average diameter ranging from 1 μm to 3 μm. These inclusions were effectively modified by rare earth elements (La, Ce, Nd).

Keywords: high-manganese austenitic steel, TWIP steel, microstructure, mechanical properties.

INTRODUCTION

Twinning-induced plasticity (TWIP) steels belong to the advanced high strength steels (AHSS) group, which are characterised by high mechanical properties [1]. As a result of optimal combination of high strength, significant ductility and the ability to absorb deformation energy, these steels are widely used in the automotive industry, especially for structural elements responsible for the passive safety of vehicles [2]. The TWIP steels are most often applied for the elements located in the controlled deformation zone [3]. Due to their high energy absorption capacity, TWIP steels can also be used as constructional materials in the applications requiring shock-resistance, including the elements resistant to explosions or earthquakes [4, 5].

The superior set of performance properties of these steels, in particular the excellent combination of strength and ductility, results from the occurrence of mechanical twinning. Deformation twins, which divide austenite grains and thus shorten the unconstrained path of dislocation movement, are formed during plastic deformation in the austenitic matrix [6]. This phenomenon leads to significant strain hardening, which allows obtaining high strength and plasticity of the material [7]. The presence of the TWIP effect is strictly related to the value of stacking fault energy (SFE), which in steels exhibiting mechanical twinning is usually equal from 20 to 60 mJ/m² [8]. TWIP steels are characterised by high concentration of manganese, most often in a range of 15–30%, stabilizing austenite along with carbon, and the presence of Si and Al, which influence the value of SFE [9]. Aluminium plays a particularly important role, as it not only increases the stacking fault energy, but also contributes to reducing the density and, consequently, the weight of the construction [10].

Pang et al. [11] investigated the behaviour of the TWIP steel containing 20% Mn during strain hardening at different strain rates (10^{-4}÷10^{3} s^{-1}). The authors showed that the strain rate has a significant influence on the morphology and number of twins formed. At a strain rate of 10^{2} s^{-1}, numerous secondary strain twins were revealed, which, in interaction with primary twins, increased the resistance to dislocation motion and the plasticity of the steel. During plastic deformation at a rate of 10^{2} s^{-1}, a significantly higher rate of twin formation was observed than during deformation at a rate of 10^{0} s^{-1}. Under quasi-static deformation conditions, the number of strain twins revealed was negligible. It was demonstrated that plastic deformation is the result of a combined interaction between strain twins and dislocation slip, which influences the hardening rate, strength, and plasticity.

TWIP steels exhibit high mechanical properties under dynamic loads conditions. It was shown in numerous studies that yield strength and tensile strength increase along with strain rate [12, 13]. It was observed that under dynamic deformation conditions, yield strength increases from about 1133 MPa to about 1430 MPa, which further boosts the ability of material to absorb energy during sudden loading [14].

Shen et al. [15,16] analysed the effect of grain size on the mechanical properties of TWIP steel containing 20% Mn and 0.6% C. The average grain size of the examined steels ranged from 3.5 to 25 µm. It was revealed that the steel with the most fine-grained microstructure (d ~ 3.5 µm) achieved tensile strength of 1930 MPa, while maintaining considerably high plasticity (reduction in area above 60%). The conducted studies showed that, at a constant strain rate, both the yield strength and the tensile strength increased significantly with decreasing grain size, while the elongation decreased slightly. For the steels with nearly identical grain size, the yield strength increased with increasing strain rate, whereas the tensile strength and elongation exhibited the opposite behaviour.

Zhang et al. [17] demonstrated that supersaturation and annealing temperature significantly affect the microstructure and mechanical properties of TWIP steel with Al, Si, V and Mo additions. A minor increase in grain size was noted due to revealed MC and M_2C type precipitations, inhibiting the increase of austenite grain size. It was shown that the ductility of TWIP steel after supersaturation, cold rolling, and subsequent annealing was significantly higher than that of the non-solution heat treatment. This was due to the fact that large MC and M_2C precipitates redissolved in the matrix after solution heat treatment and were not retained in the structure subjected to subsequent annealing. After supersaturation, plastic deformation and subsequent annealing at a temperature of 800°C, the steel obtained optimal mechanical properties (YS ~ 877 MPa, UTS ~ 1457 MPa, UEl ~ 46%).

Tewary et al. [18] observed that the tensile strength and elongation of TWIP steel decrease along with increasing annealing time and temperature, which is related to the increase in grain size. The optimal combination of strength and ductility was obtained for partially recrystallised samples annealed at 700°C for 30 min (UTS ~ 859 MPa, UEl ~ 37%) and annealed at 900°C for 30 min (UTS ~ 708 MPa, UEl ~ 63%). Tian et al. [19] examined the Fe-22Mn-0.6C TWIP steel with ultrafine-grained microstructure. A 12 mm thick charge (initial grain size ~21 µm) was subjected to multi-stage cold rolling. In the first stage, the thickness was reduced to 8 mm, in the second, to 5 mm, in the third, to 3 mm, and in the fourth, to 1 mm (with a total thickness reduction of 92%). After each rolling stage, the sheet was annealed at 600°C for 10 minutes.

After these treatments (minimum average grain size was equal about 550 nm), the steel demonstrated yield strength of approximately 793 MPa, tensile strength of approximately 1247 MPa and uniform elongation of approximately 47%, ensuring a favourable balance between strength and plastic properties.

The aim of the research was to evaluate the effect of supersaturation temperature on the microstructure and mechanical properties of high-manganese austenitic TWIP steel.

MATERIALS AND METHODS

The experiments described in the paper were performed on austenitic steel with a high manganese content, characterised by TWIP effect, containing 0.054% C, 24.4% Mn, 0.004% P, 0.006% S, 3.5% Si, 1.6% Al, 0.029% Nb, 0.075% Ti and 0.0040% N. The impact of main alloying elements on the strengthening mechanisms, microstructure and selected properties is summarised in Table 1. A 26 kg melt was carried out in a Balzers VSG-50 induction furnace, which is part of the equipment at the Łukasiewicz Research Network – Centre for Metallurgical Technologies.

Non-metallic inclusions were modified using rare-earth metals, which were introduced into the liquid steel as mischmetal. This process was intended to change the chemical composition, morphology, and distribution of the inclusions, which favourably affects the material's functional properties, particularly ductility and fracture toughness. After completing the metallurgical process, the ingots were subjected to preliminary hot plastic processing. They were transformed into flat bars measuring 20 × 180 mm using the open-die forging method, which allowed for a more uniform material structure, reduced potential discontinuities, and elimination of internal defects, improves plasticity and impact strength.

Flat bars, after austenitising at a temperature of 1200°C, were subsequently subjected to hot rolling in six passes to a 6.5 mm thick sheet, with the rolling finish temperature equal 900°C. A detailed program of flat bar rolling was described in [20]. Supersaturation at temperatures of 900°C, 1000°C and 1100°C with subsequent water cooling was carried out on 20 × 15 × 6 mm samples. The mechanical properties of the investigated steel were determined by static tensile testing using flat specimens with a cross-section of 6.3 × 3 mm and a gauge length of 25 mm. The experiments were performed in accordance with the requirements of the ASTM standard [21], ensuring repeatability and reliability of the obtained results. Microstructural characterisation, performed after supersaturation and subsequent tensile test, was carried out using a LM, SEM, TEM and X-ray-based techniques. Such a multiscale approach enabled a comprehensive analysis of the steel's structural features and phase constituents. Metallographic observations were performed on the specimens etched with nitric acid and ethanol solution using an optical microscope (AXIO Observer). Examinations were performed at magnifications ranging from 100× to 1000×, allowing for the assessment of general microstructural features, including grain size and distribution. Grain size measurements were carried out using the secants method with the requirements of the ASTM standard [22], supported by the AXIO Vision image analysis computer program. Microstructural details and fracture surface analyses of the specimens were examined using SEM (Zeiss SUPRA 35). The SEM investigations were conducted on nital-etched samples at an accelerating voltage of 20 kV, with magnifications ranging from 1000× up to 30 000×, providing high-resolution insight into the morphology and distribution of microstructural constituents. EBSD studies were performed in the same device, using a scanning step from 0.12 to 1.5 µm. Data processing was executed using the TSL®OIM software [23]. After standard grinding and polishing, the samples were ion polished on a GATAN 682 polishing machine for approximately 1.5 h at the voltage of 2 keV. Lamellae for transmission electron microscopy (TEM) examinations were prepared using the focused ion beam (FIB) method. The process involved applying a protective layer, cutting the lamellae with an ion beam, transferring and mounting them on a TEM grid, and subsequent final thinning with low-current ions. As a result of the FIB use, it was possible to obtain lamellae with thickness of tens of nanometres, suitable for observation in transmission electron microscopy. Microstructure studies were carried out in TEM, set to 300 kV and featuring a Schottky-type field emission gun. Chemical composition of revealed precipitations was determined with the use of the EDS method. X-ray phase analysis was performed in the Bragg-Brentano geometry using an X'Pert PRO diffractometer. A Co anode X-ray tube was employed (U = 40 kV; I = 30 mA), ensuring sufficient intensity and resolution of the diffraction signal. Data acquisition was conducted using a step-scanning method, with a step size of 0.05° in terms of the 2θ

Table 1. The influence of individual elements on the strengthening mechanisms, microstructure and selected properties of investigated TWIP steel

Effect	C	Mn	Si	Al	Nb	Ti	N
Austenite stability	+	+		+			+
Solid solution strengthening austenite			+	+			
Fine-grained microstructure					+	+	
ε-martensite refinement			+				
Hot ductility				−	+	+	

angle. The diffraction patterns were recorded over a range from 20° to 100°, with a counting time of 50 seconds per step, which allowed for precise detection of diffraction peaks and improved signal-to-noise ratio.

RESULTS

The microstructure of the tested TWIP austenitic steel, in which deformation twins are clearly observed, after supersaturation at temperatures of 900°C, 1000°C, and 1100°C is shown in Figure 1. Analysis of the obtained microstructural images indicates that with increasing solution heat treatment temperature, a systematic increase in austenite grain size occurs, which is a characteristic effect of the intensified diffusion processes and grain boundary migration at elevated temperatures. The samples subjected to supersaturation with water cooling from temperatures of 900°C and 1000°C are characterised by a fine-grained austenitic structure with a relatively uniform grain size distribution. The average austenite grain diameter under these conditions is 15.0 μm at 900°C and 20.4 μm at 1000°C, respectively, indicating limited grain growth within the analysed temperature range.

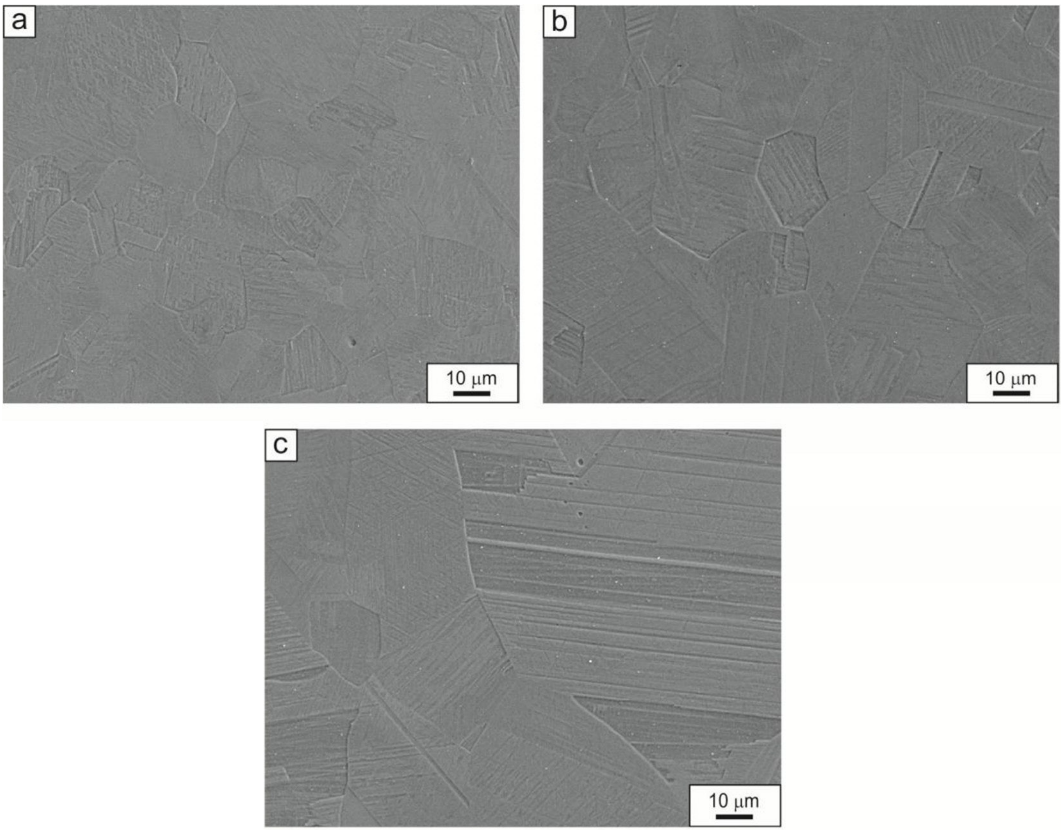

Figure 1. Microstructure of the examined steel with twins in austenite grains after supersaturation at a temperature: a) 900°C, b) 1000°C, c) 1100°C followed by water cooling

A distinct change in the microstructure is observed after the solution temperature exceeds 1000°C, as shown in Figure 2. In the case of the samples solution treated at 1100°C, also with water cooling, intensive austenite grain growth occurs. The average grain diameter then reaches 131.6 µm, indicating a significant acceleration of austenite grain growth.

In line with the Hall-Petch relationship [24, 25], the strength of polycrystalline materials can be increased via grain refinement. Linear relationship between stress and grain size (average grain diameter – d) for the tested steel, is shown in Figure 3.

The results of the static tensile test are summarised in Table 2. Average austenite grain diameter significantly impacts obtained mechanical properties. The highest set of mechanical properties ($YS_{0.2}$ ~ 485 MPa and UTS ~ 797 MPa) was achieved for the samples previously subjected to supersaturation at a temperature of 900°C with water cooling (d ~ 15.0 µm). Increasing the supersaturation temperature to 1000 °C (d ~ 20.4 µm) results in a slight decrease in strength properties: $YS_{0.2}$ to about 463 MPa and UTS to about 767 MPa. The lowest mechanical properties were obtained for the samples subjected to supersaturation at a temperature of 1100°C with water cooling (d ~ 131.6 µm). In the applied supersaturation temperature range (900–1100°C), the elongation of samples increased from approx. 39% to about 49%, while the reduction in area from approx. 43% to about 51%.

The data set together in Table 2 also show that the examined steel has low values of the $YS_{0.2}$/UTS ratio (from 0.61 for the supersaturation temperature of 900°C to 0.52 for the supersaturation temperature of 1100°C), which is particularly advantageous from hot rolling process the point of view of. Noteworthy are also high values of the UTS×UEl product (from 31 003 MPa×% to 32 209 MPa×%). The microstructures of tested TWIP steel, after supersaturation at temperatures of 900°C and 1100°C followed by tensile testing, are shown in Figure 4. After plastic deformation to fracture, the examined steel samples display austenitic microstructure with numerous twins and slip bands. The slip bands are most frequently located in larger grains, often intersecting each other due to slip occurring in at least two systems.

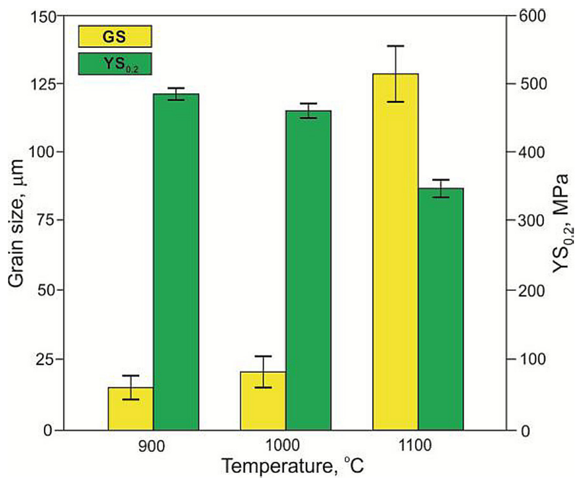

Figure 2. Effect of supersaturation temperature on grain size (GS) and yield strength ($YS_{0.2}$)

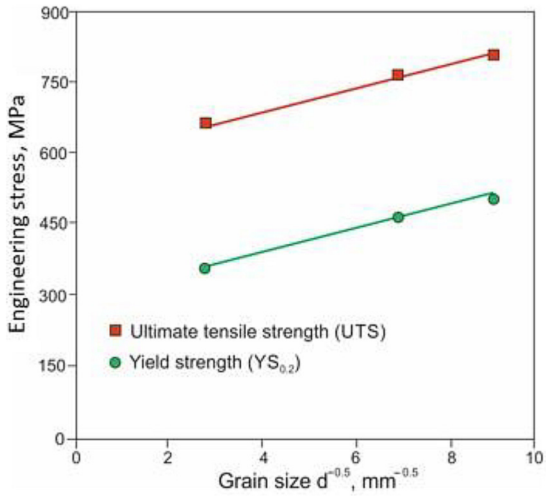

Figure 3. Dependence of grain sizes on UTS and $YS_{0.2}$ of investigated TWIP steel

X-ray diffraction analysis revealed the presence of ε-martensite (Figure 5). The presence of ε martensite in the microstructure of the steel subjected to tension after prior supersaturation at temperatures ranging from 900°C to 1100°C with water cooling, was confirmed by EBSD tests. The EBSD analysis results, after supersaturation at a temperature of 1000 C and subsequent tensile testing, are presented in Figure 6.

The average volume fraction of ε martensite (marked in green in Figure 6b) after tension is equal 8.4%. The minor fraction of this phase – not changing significantly across the applied supersaturation temperature range – does not affect the mechanical properties of the steel studied. Lamellae of ε martensite occur locally, mainly in highly deformed grains where two slip bands intersect. The ε martensite lamellae are indicated by yellow ellipses in Figure 6c. The ε martensite

Table 2. Influence of supersaturation temperature on grain size and strength and plastic properties of the tested steel with TWIP effect

Supersaturation temperature, °C	Grain size, μm	$YS_{0.2}$, MPa	UTS, MPa	$YS_{0.2}$/UTS	UEl, %	RA, %	UTS·UEl, MPa·%
900	15.0	485	797	0.61	38.9	43.0	31 003
1000	20.4	463	767	0.60	43.2	46.3	33 134
1100	131.6	345	656	0.52	49.1	50.8	32 209

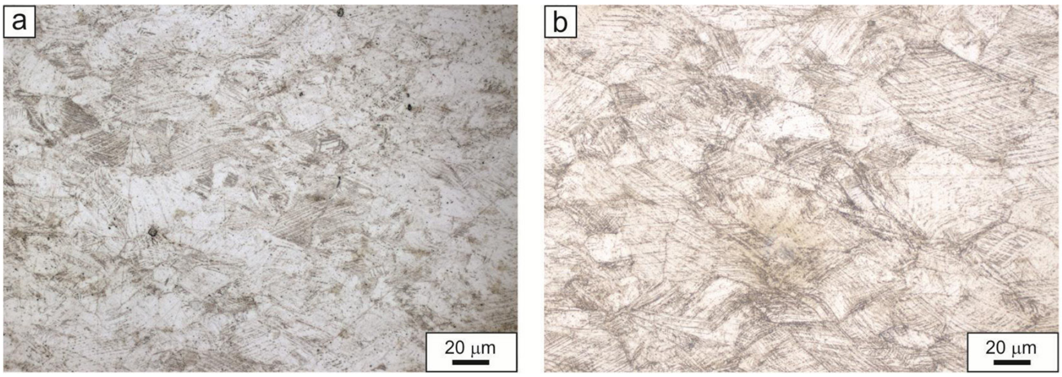

Figure 4. Microstructure after supersaturation at temperature: 900°C (a) and 1100°C (b) with water cooling and subsequent tensile testing

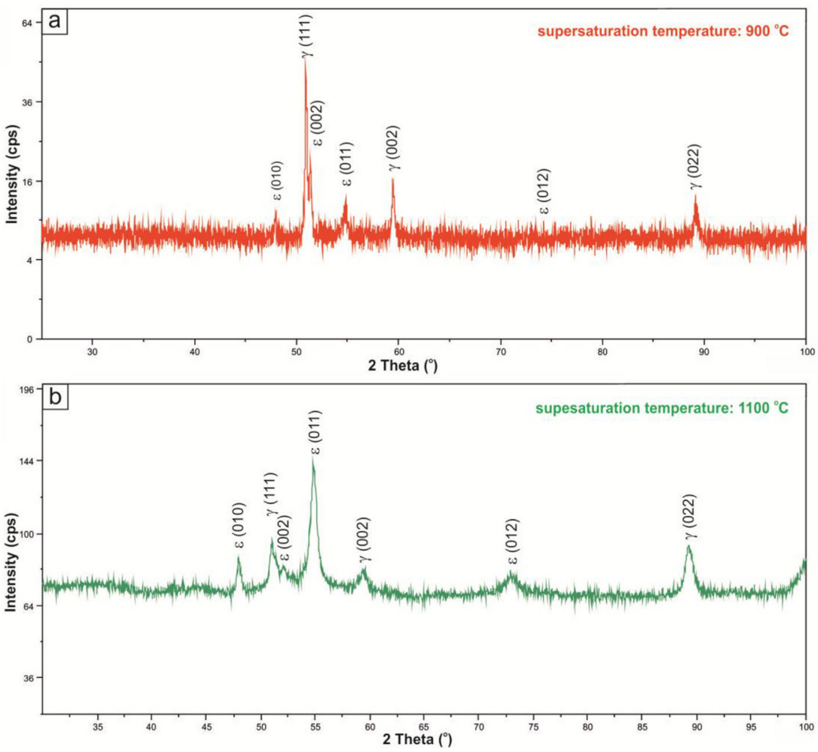

Figure 5. X-ray diffraction patterns of the tested steel after supersaturation in water and subsequent tensile testing; supersaturation temperature: 900°C (a) and 1100°C (b)

was also observed in TWIP austenitic steel with a chemical composition similar to the investigated steel, as reported in [26, 27].

The results of microstructural examination of the lamellae, taken from samples after tensile testing and prior supersaturation, using a transmission electron microscope, are presented in Figures 7 and 8. Dispersive carbides of the (Ti,Nb)C type, located mainly at the austenite grain boundaries, were identified in the microstructure (Figure 7).

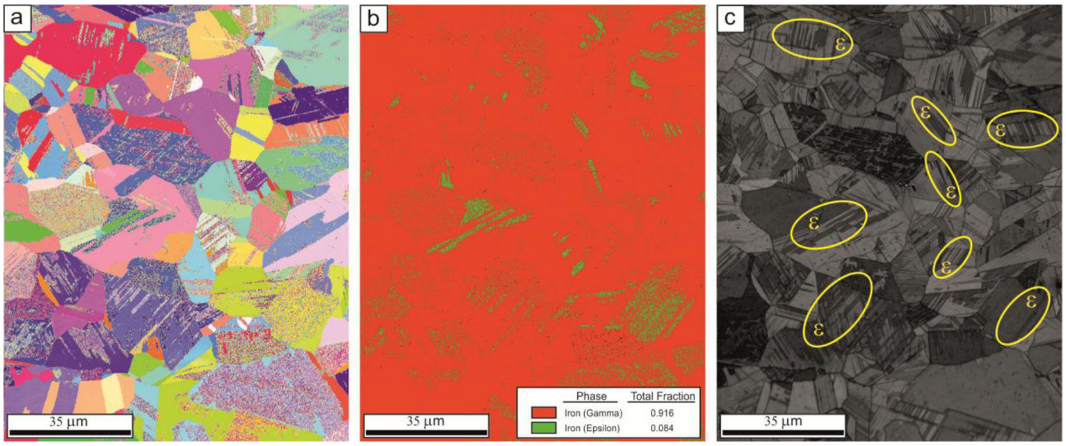

Figure 6. Microstructure after supersaturation at a temperature of 1000°C and subsequent tensile testing: distribution map of grains with different crystallographic orientation (a), areas of ε martensite presence highlighted in green (b), and image quality map (c)

Complex (Ti,Nb)C type carbides, with an average size ranging from 3 nm to 10 nm, were detected using energy dispersive spectroscopy (EDS). Microanalysis of these precipitations revealed that, in most cases, they are particles with the approximate chemical formula $(Ti_{0.5}Nb_{0.5})C$. The studies conducted in transmission electron microscope also revealed complex carbonitrides precipitations of the (Ti,Nb)(C,N) type (Figure 8), with an average size of 20 nm to 50 nm.

The examined surfaces of the samples subjected to static tensile testing after supersaturation at temperatures of 900°C and 1100°C, are shown in Figure 9. Examinations confirmed the ductile nature of the fractures. The topography of the fracture surface is characterised by the presence of many craters and voids of varying sizes. The craters in the sample solution heat-treated at a temperature of 1100°C (Figure 9b) are notably larger than those in the sample subjected to supersaturation at a temperature of 900°C (Figure 9a). Non-metallic inclusions are present on the examined surfaces – they are most frequently globular, located inside the craters (Figure 9b). The diameter of the observed non-metallic inclusions ranged from 1 µm to 3 µm. In most cases, the non-metallic inclusions were identified as complex sulphide-oxide type effectively modified by rare-earth metals (La, Ce, Nd) – Figure 10.

DISCUSSION

The microstructures shown in Figure 1 and the data set together in Figure 2 indicate that the supersaturation temperature has a significant impact on the austenite grain size, which determines the mechanical properties of the tested TWIP steel. The samples supersaturated from a temperature of 900°C have a fine-grained structure with an average grain diameter of ~ 15 µm (Figures 1a and 2). Increasing the supersaturation temperature by 100°C does not cause significant grain growth (~ 20 µm) – (Figures 1b and 2). However, the consequence of supersaturation of samples from a temperature of 1100°C is obtaining a coarse-grained structure (d ~ 132 µm) with a considerable quantity of twins (Figure 1c). Comparable results were obtained by Ueji et al. [28, 29], Dini et al. [30] and Yuan et al. [31], who investigated the role of grain size in high-manganese TWIP steels. According to the data in [32], the energy required to form deformation twins must be greater than the critical stress. Considering that the critical stress needed to form deformation twins increases as grain size decreases, deformation twins are less likely to form in fine-grained microstructures and more likely in coarse-grained microstructures [30, 33, 34]. This explains the increase in elongation with increasing grain size (Table 2).

The tested steel demonstrates a favourable combination of mechanical properties, particularly after supersaturation at temperatures of 900°C and 1000°C. The highest strength properties ($YS_{0.2}$ ~ 485 MPa and UTS ~ 797 MPa) were obtained for the samples previously supersaturated from a temperature of 900°C (d ~ 15 µm). As a result of increasing the supersaturation temperature to 1100°C (d ~ 132 µm), the strength

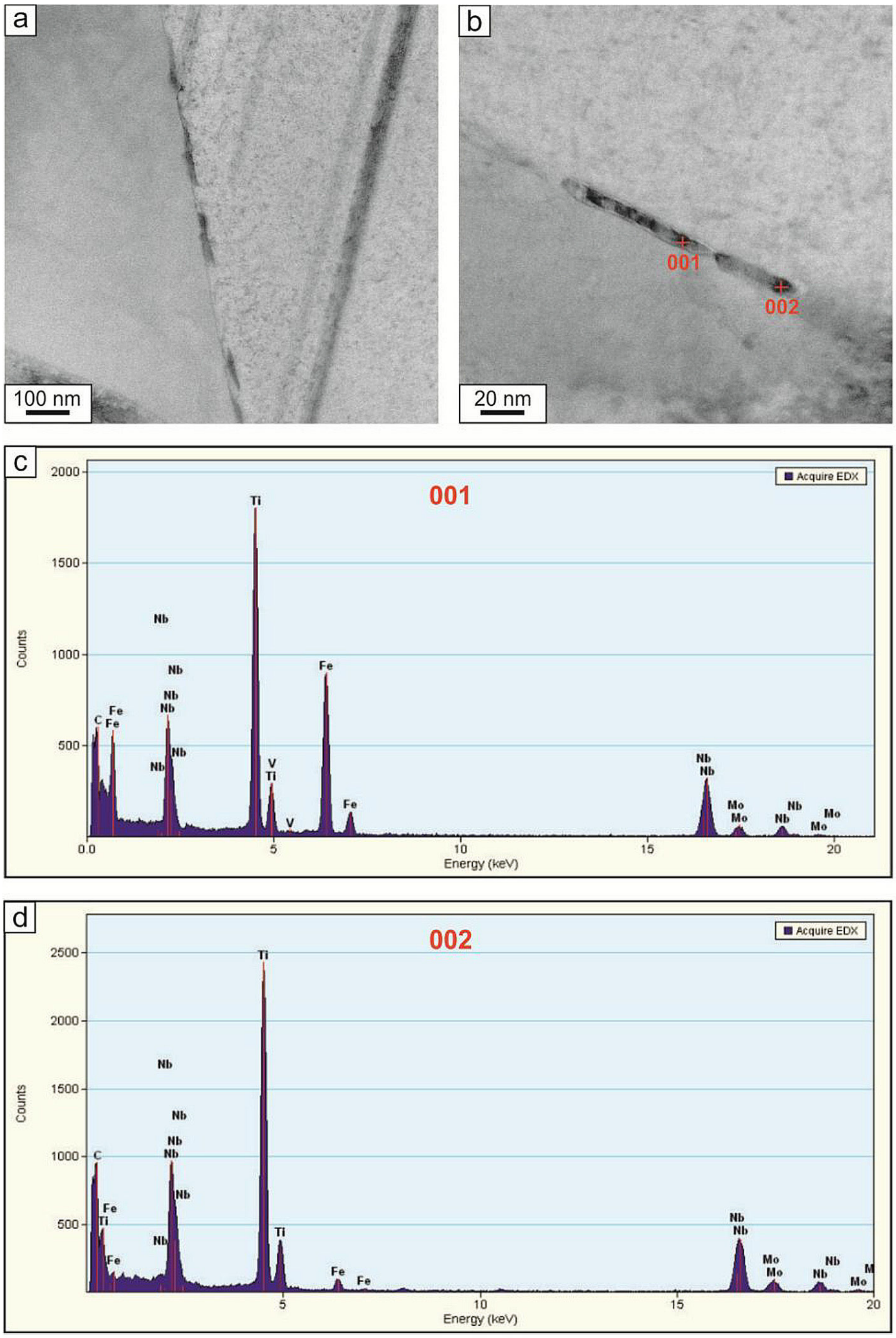

Figure 7. (Ti,Nb)C type carbides at the austenite grain boundary (a, b), EDS spectrum from point "001" (c), EDS spectrum from point "002" (d); supersaturation temperature of 900°C

properties decreased while the plastic properties increased (Table 2). A similar trend in the change of mechanical properties was observed by Lee et al. [35] when investigating steel containing 24% Mn, solution heat treated at temperatures of 800°C and 1100°C, as well as by Yuan et al. [31] who tested steel containing 25% Mn after supersaturation in water at temperatures ranging from 700°C to 1000°C. The observed increase in plasticity with simultaneous decrease $YS_{0.2}$ and UTS (with increasing supersaturation temperature), is typical for TWIP steels and is attributed to the effect of deformation twins [36], and more specifically – a significant increase in the number of deformation twins. As demonstrated by Dini [30], El-Danaf [32], De Cooman [36], and Bouaziz [37], as grain size decreases, the stress required to form strain twins increases. Therefore, grain refinement affects the kinetics of twin formation. Although too small a grain may hinder twin formation,

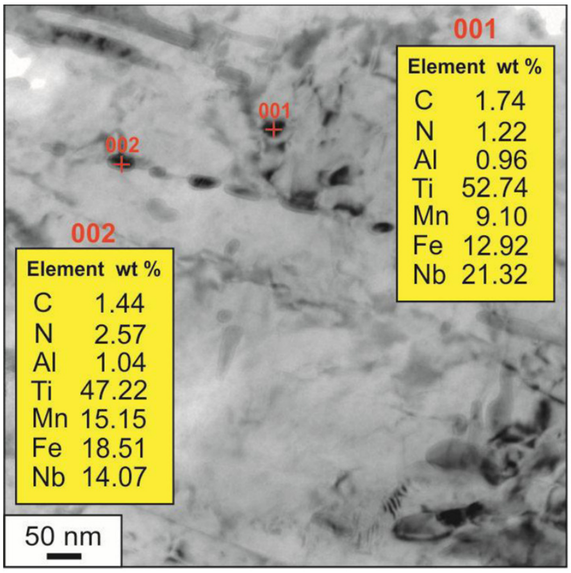

Figure 8. (Ti,Nb)(C,N) type carbonitrides; supersaturation temperature of 1000°C

optimal refinement will provide the best compromise between strength and elongation.

The research carried out showed that the analysed steel exhibits low values of the $YS_{0.2}$/UTS ratio (from 0.61 to 0.52), which indicates an intensive course of strain hardening occurring in the range of uniform elongation of the samples. Comparable values were obtained in [38] for austenitic steel containing 30% Mn. Moreover, the examined steel, within the supersaturation temperature range of 900°C to 1100°C, is characterised by high values of the UTS×UEl (from 31003 MPa×% to 32209 MPa×%), which determines the stability of deformation conditions during potential sheet stamping process.

The presence of ε martensite was identified in the tested steel, with its volume fraction – regardless of the supersaturation temperature – at approximately 8%. This phase was detected both by X-ray examination (Figure 5) and by the EBSD method (Figure 6). The occurrence of ε martensite in the examined steel is likely attributable to low aluminium content, which leads to an increase in the tendency of the γ → ε transformation occurring during cooling after hot working. The presence of ε martensite with similar morphology in high-manganese TWIP steels has also been reported in [26, 27, 39, 40].

Introduction of Nb (0.029%) and Ti (0.075%) microadditions to the tested steel was intended to promote the formation of carbides and carbonitrides during hot working and thus creating a fine-grained microstructure [41–43]. Dispersive (Ti,Nb)C carbides were identified in the examined steel – Figure 7 as well as (Ti,Nb)(C,N) carbonitrides – Figure 8. The mentioned particles are responsible for inhibiting the growth of austenite grains and thus for obtaining a fine-grained microstructure. Microstructural observations made using transmission electron microscopy were fully consistent with the grain size results. The specimens subjected to supersaturation at temperatures of 900°C and 1000°C maintain a fine-grained microstructure (d ~ 15–20 μm) due to the presence of dispersive (Ti,Nb)C and (Ti,Nb)(C,N) precipitations. At a temperature of 1100°C, a significant volume fraction of Nb and Ti remains dissolved in the solid solution, resulting in the development of a coarse-grained microstructure (Figure 1c).

The research conducted in scanning electron microscope enabled the determination of the effect of supersaturation temperature on the surface morphology of fractured samples after performed tensile testing. The observations revealed

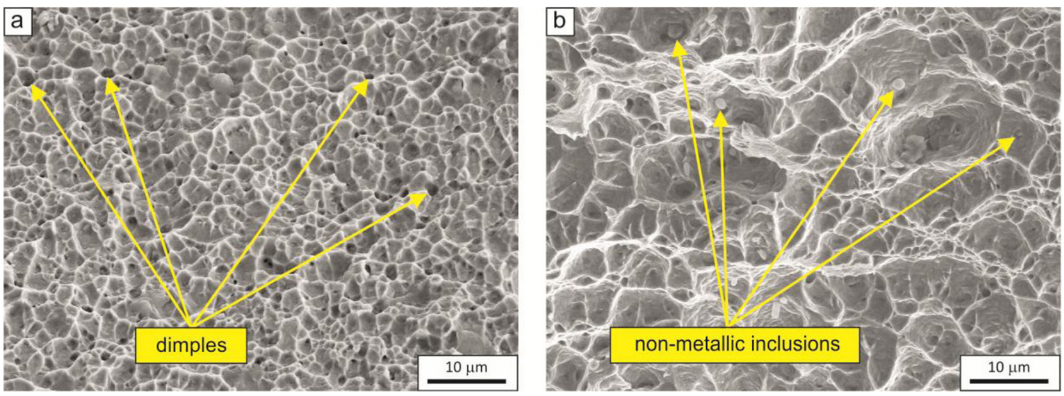

Figure 9. Fractures of samples after supersaturation and subsequent tensile testing: a – supersaturation temperature of 900 °C, b – supersaturation temperature of 1100°C

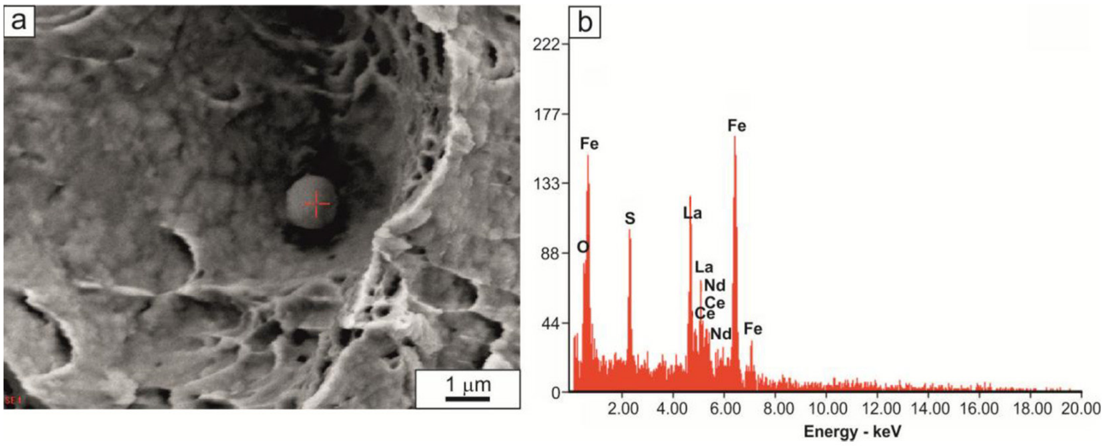

Figure 10. Globular non-metallic sulphide-oxide type inclusion, modified with La, Nd and Ce, on the fracture surface of sample after supersaturation and subsequent tensile testing: a – view of inclusion; b – spectrometric spectrum of non-metallic inclusion; supersaturation temperature of 1000°C

that, irrespective of the supersaturation temperature, the fractures in the studied steel were ductile with numerous craters and voids, the size of which increased significantly in the case of samples solution heat treated at a temperature above 1000°C. This corresponds to significant growth of austenite grains after this temperature is exceeded. Small (from 1 µm to 3 µm), globular non-metallic inclusions were detected on the fracture surface (Figures 9b and 10a). In most cases, the non-metallic inclusions were identified as complex sulphide-oxide type modified by rare-earth metals (La, Ce, Nd).

CONCLUSIONS

The tests conducted on high-manganese austenitic TWIP steel allow the following conclusions to be drawn:

- an increase of the temperature (from 900 °C to 1100 °C), leads to growth of austenite grains from approx. 15 µm to approx. 132 µm,
- within the applied range of supersaturation temperature, a decrease in $YS_{0.2}$ and UTS is observed ($YS_{0.2}$ from approx. 485 MPa to about 345 MPa, and UTS from approx. 797 MPa to about 656 MPa) whilst plastic properties increase (EUl from approx. 39% to about 49%, and the reduction in area from approx. 43% to about 51%),
- low values obtained for the $YS_{0.2}$/UTS ratio (from 0.61 to 0.52) indicate an intensive course of strain hardening, occurring within the uniform elongation range of samples,
- the presence of ε martensite was revealed in the tested steel, with its portion – regardless of the supersaturation temperature – equal approximately 8%,
- the presence of dispersive (Ti,Nb)C carbides and (Ti,Nb)(C,N) carbonitrides, mainly located at the austenite grain boundaries, ensures fine-grained microstructure,
- after tensile test, samples have ductile fractures with numerous craters, the size of which increases significantly after exceeding supersaturation temperature of 1000 °C,
- non-metallic inclusions (in most case sulphide-oxide type) observed on the fracture surface, effectively modified with rare earth metals (La, Ce, Nd), are globular in shape,
- proposed supersaturation temperature is 900 °C because of optimal combination of mechanical properties ($YS_{0.2}$ = 485 MPa, UTS = 797 MPa, RA = 43%).

Acknowledgements

This research was funded by a second-degree pro-quality grant awarded by the Rector of Silesian University of Technology (grant no. 10/010/RGJ25/1232).

REFERENCES

1. Bouaziz O., Allain S., Scott C.P., Cugy P., Barbier D. High manganese austenitic twinning induced plasticity steels: A review of the microstructure properties relationships. Current Opinion in Solid State

and Materials Science 2011; 15(4): 141–168. https://doi.org/10.1016/j.cossms.2011.04.002

2. Cai W., Wang C., Sun C. Microstructure evolution and fracture behaviour of TWIP steel under dynamic loading. Materials Science and Engineering A 2022; 851: 1–11. https://doi.org/10.1016/j.msea.2022.143657
3. De Cooman B.C., Estrin Y., Kim S.K. Twinning-induced plasticity (TWIP) steels. Acta Materialia 2018; 142: 283–362. https://doi.org/10.1016/j.actamat.2017.06.046
4. Feng X.C., Liu X.Y., Bai S.X., Tang Y., Ye Y. Investigation of dynamic tensile mechanical responses and deformation mechanism at high strain rates in a TWIP steel. Journal of Materials Research and Technology 2023; 26: 639–653. https://doi.org/10.1016/j.jmrt.2023.07.241
5. Deng, J.H., Li C.W., Wang Z.Y., Tong W., Wu Q.Y. Effect of post-weld heat treatment on microstructure and mechanical properties of twinning-induced plasticity (TWIP) steel joints. Materials Today Communications 2024; 40: 1–11. https://doi.org/10.1016/j.mtcomm.2024.109720
6. Xinchang F., Xiyue L., Shuxin B., Yu T., Yicong Y. Investigation of dynamic tensile mechanical responses and deformation mechanism at high strain rates in a TWIP steel. Journal of Materials Research and Technology 2023; 26: 630–653. https://doi.org/10.1016/j.jmrt.2023.07.241
7. Mejía I.,Hernández-Belmontes H., Maldonado C. Weldability of high-Mn austenitic twinning-induced plasticity (TWIP) steel microalloyed with Nb. Materials Research Society Advances 2018: 3899–3908. https://doi.org/10.1557/adv.2018.108
8. Fajardo S., Llorente I., Jimenez J.A., Bastidas J.M., Bastidas, D.M. Effect of Mn additions on the corrosion behaviour of TWIP Fe-Mn-Al-Si austenitic steel in chloride solution. Corrosion Science 2019; 154: 246–253. https://doi.org/10.1016/j.corsci.2019.04.026
9. Chowdhury P., Canadinc D., Sehitoglu H. On deformation behavior of Fe-Mn based structural alloys. Materials Science and Engineering A 2017; 122: 1–28. https://doi.org/10.1016/j.mser.2017.09.002
10. Wang D., Huang L., Wang K. et el. Microstructure and mechanical properties of a novel twinning induced plasticity steel with two different grain morphologies. Journal of Materials Research and Technology 2023; 24: 3746–3758. https://doi.org/10.1016/j.jmrt.2023.04.080
11. Pang Q.H., Xu M., Mi Z.L. et al. Microstructure evolution of ultra-high-strength twinning-induced plasticity (TWIP) steel under dynamic loading, Journal of Iron and Steel Research International 2021; 28: 66–75. https://doi.org/10.1007/s42243-020-00457-2
12. Yang J., Liu X., Tang Y., Bai S., Ye Y., He M., Xia M. Dynamic mechanical properties and deformation mechanisms of lightweight high-strength TWIP Steel. Buildings 2025; 15(6): 897. https://doi.org/10.3390/buildings15060897
13. Guo P.C., Qian L.H., Meng J.Y., Liu S., Zhang F. Effect of Al on the low cycle fatigue deformation behavior and microstructure evolution of Fe-22Mn-0.6C TWIP steel. Journal of Materials Research and Technology 2024; 30: 2086–2098. https://doi.org/10.1016/j.jmrt.2024.03.221
14. Canadinc D., Sehitoglu H., Maier, H.J., Niklasch D., Chumlyakov Y. Orientation evolution in Hadfield steel single crystals under combined slip and twinning. International Journal of Solids and Structures 2007; 44: 34–50. https://doi.org/10.1016/j.ijsolstr.2006.04.011
15. Shen Y.F., Jia N., Wang Y.D., Sun X., Zuo L., Raabe D. Suppression of twinning and phase transformation in an ultrafine grained 2 GPa strong metastable austenitic steel: Experiment and simulation. Acta Materialia 2015; 97: 305–315. https://doi.org/10.1016/j.actamat.2015.06.053
16. Shen Y.F., Jia N., Misra R.D.K., Zuo L. Softening behavior by excessive twinning and adiabatic heating at high strain rate in a Fe–20Mn–0.6C TWIP steel. Acta Materialia 2016; 103: 229–242. https://doi.org/10.1016/j.actamat.2015.09.061
17. Zhang J., Bai T., Fan W., Zhang G., Zhang W., Yang Y., Hao H. Microstructure and mechanical properties of a new TWIP steel under different heat treatments. Materials 2024; 17(2080): 2–14. https://doi.org/10.3390/ma17092080
18. Tewary N.K., Ghosh S.K., Mandal A., Chakrabarti D., Chatterjee S. Effect of annealing on the microstructure, texture and mechanical properties of a dual-phase ultrahigh-strength TWIP steel. Metallurgical and Materials Transactions A 2020; 51: 4483–4498. https://doi.org/10.1007/s11661-020-05851-9
19. Tian Y.Z., Bai Y., Chen M.C., Shibata A., Terada D., Tsuji N. Enhanced strength and ductility in an ultrafine-grained Fe-22Mn-0.6C austenitic steel having fully recrystallized structure, Metallurgical and Materials Transactions A 2014; 45: 5300–5304. https://doi.org/10.1007/s11661-014-2552-2
20. Opiela M., Fojt-Dymara G. Effect non-metallic inclusions on the hot ductility of high-Mn steels. Advances in Science and Technology. Research Journal 2023; 17(3): 19–30. https://doi.org/10.12913/22998624/162702
21. ASTM E8/E8M-25. Standard test method for tension testing of metallic materials.
22. ASTM E112-10. Standard test methods for determining average grain size.

23. TSL®OIM Analysis for Windows. User's Guide. Version 4.3. EDAX TSL, TexSem Laboratories Inc., Draper, USA, 2004.
24. Petch J.N. The cleavage strength of polycrystals. Journal of the Iron and Steel Institute 1953; 5: 25–28.
25. Sato K., Ichinose M., Hirotsu Y. Effects of deformation induced phase transformation and twinning on the mechanical properties of austenitic Fe-Mn-Al alloys. ISIJ International 1989; 29(10): 868–877. https://doi.org/10.2355/isijinternational.29.868
26. Phiu-on K., Bleck W., Schwedt A., Mayer J. Effects of solution treatment and test temperature on tensile properties of high Mn austenitic steels. Steel Research International 2009; 80(1): 29–38. https://doi.org/10.2374/SRI08SP120
27. Sevsek S., Brasche F., Molodov D.A., Bleck W. On the influence of grain size on the TWIP/TRIP-effect and texture development in high-manganese steels. Materials Science and Engineering A 2019; 754: 152–160. https://doi.org/10.1016/j.msea.2019.03.072
28. Ueji R., Tsuchida N., Terada D., Tsuji N., Tanaka T., Takemura A., Kunishige K. Tensile properties and twinning behavior of high manganese austenitic steel with fine-grained structure. Scripta Materialia 2008; 59: 963–966. https://doi.org/10.1016/j.scriptamat.2008.06.050
29. Ueji R., Tsuchida N., Fujii H., Kondo D., Kunishige K. Effect of grain size on tensile properties of TWIP steel. Journal of the Japan Institute of Metals and Materials 2007; 71: 815–821. https://doi.org/10.2320/jinstmet.71.815
30. Dini G., Najafizadeh A., Ueji R., Monir-Vaghefi S.M. Tensile deformation behavior of high manganese steel: the role of grain size. Materials and Design 2010; 31: 3395–3402. https://doi.org/10.1016/j.matdes.2010.01.049
31. Yuan X., Chen L., Zhao Y., Di H., Zhu F. Dependence of grain size on mechanical properties and microstructures of high manganese austenitic steel. Procedia Engineering 2014; 81: 143–148. https://doi.org/10.1016/j.proeng.2014.09.141
32. El-Danaf E., Kalidini S.R., Doherty R.D. Influence of grain size and stacking-fault energy on deformation twining in fcc metals. Metallurgical and Materials Transactions A 1999; 30: 1223–1233. https://doi.org/10.1007/s11661-999-0272-9
33. Huang A., Fensin S.J., Meyers M.A. Strain-rate effects and dynamic behavior of high entropy alloys. Journal of Materials Research and Technology 2023; 22: 307–347. https://doi.org/10.1016/j.jmrt.2022.11.057
34. Opiela M., Fojt-Dymara G., Grajcar A., Borek W. Effect of grain size on the microstructure and strain hardening behavior of solution heat-treated low-C high-Mn steel. Materials 2020; 13(7) 1–13. https://doi.org/10.3390/ma13071489
35. Lee S.I., Lee S.Y., Han J., Hwang B. Deformation behavior and tensile properties of an austenitic Fe-24Mn-4Cr-0.5C high-manganese steel: effect of grain size. Materials Science and Engineering A 2019; 742: 334–343. https://doi.org/10.1016/j.msea.2018.10.107
36. De Cooman B.C., Estrin Y., Kim S.K. Twinning-induced plasticity (TWIP) steels. Acta Materialia 2018; 142: 283–362. https://doi.org/10.1016/j.actamat.2017.06.046
37. Bouaziz O., Allain S., Scott C. Effect of grain and twin boundaries on the hardening mechanisms of twinning-induced plasticity steels. Scripta Materialia 2008; 58: 484–487. https://doi.org/10.1016/j.scriptamat.2007.10.050
38. Sevsek S., Brasche F., Haase C., Bleck W. Combined deformation twinning and short-range ordering causes serrated flow in high-manganese steels. Materials Science and Engineering A 2019; 746: 434–442. https://doi.org/10.1016/j.msea.2019.01.042
39. De Cooman B.C. Structure-properties relationship in TRIP steels containing carbide-free bainite. Current Opinion in Solid State & Materials Science 2004; 8: 285–303. https://doi.org/10.1016/J.COSSMS.2004.10.002
40. Wang H., Yang P., Mao W., Lu F. Effect of hot deformation of austenite on martensitic transformation in high manganese steel. Journal of Alloys and Compounds 2013; 558: 26–33. https://doi.org/10.1016/j.jallcom.2012.12.032
41. Opiela M., Grajcar A. Microstructure and anisotropy of plastic properties of thermomechanically-processed HSLA-type steel plates. Metals 2018; 8(5): 1–15. https://doi.org/10.3390/met8050304
42. Mejia I., Salas-Reyes A.E., Calvo J., Cabrera J.M. Effect of Ti and B microadditions on the hot ductility behavior of a high-Mn austenitic Fe-23Mn-1.5Al-1.3Si-0.5C TWIP steel. Materials Science and Engineering A 2015; 648: 311–329. https://doi.org/10.1016/j.msea.2015.09.079
43. Qaban A., Mintz B., Kang S.E., Naher S. Hot ductility of high Al TWIP steels containing Nb and Nb-V. Materials Science and Technology 2017; 33: 1645–1656. https://doi.org/10.1080/02670836.2017.1309097